ChemPubSoc Europe

DOI: 10.1002/slct.201801234

Chemistry SELECT Full Papers

Materials Science inc. Nanomaterials & Polymers

One-Pot Synthesis of Au Embedded ZnO Nanorods Composite Heterostructures with Excellent Photocatalytic Properties

Krishna Kanta Haldar,*[a] Rathindranath Biswas,[a] Swati Tanwar,[b] Tapasi Sen,[b] and Jouko Lahtinen[c]

Here, we have designed a noble composite nanostructure by embedding gold (Au) nanoparticles into zinc oxide (ZnO) nanorods surface in one pot synthesis as a photocatalyst. The formation the composite nanostructure was confirmed by X-ray diffraction, X-ray photoelectron spectroscopy (XPS), field emission scanning electron microscopy and transmission electron microscopy investigations. Microscopic studies suggest that spherical Au nanoparticles are nucleated on the ZnO nanorods surface. XPS shows shifting of peak positions towards higher binding energy which indicates charge transfer from ZnO to Au in the composite nanostructures. This is unambiguously confirmed by the steady state spectroscopic studies. It was found that 95.7% (1.8×10^{-5} mM) of Methylene blue dye is degraded by the composite nanostructure after 140 min under UV light illumination and the apparent rate constant was found to be 0.015 min^{-1}. This new class of Au nanoparticles embedded ZnO nanorods composite nanostructure opens up new possibilities in photocatalytic, solar energy conversion, photovoltaic, and other new emerging applications.

1. Introduction

Photocatalytic degradation of organic pollutants employing semiconductors nanocrystals has been broadly studied to solve energy and environmental problems.[1] In general, the photoinduced charge separation efficiency is lower for semiconductor nanomaterials for its fast recombination process.[2] For efficiently energy harvesting, the photoinduced electrons and holes of nanomaterial must be separated to reduce the recombination between them. There are various studies that have explored the charge carrier dynamics of semiconductor materials, for example, the addition of suitable electron acceptors, like noble metals,[3–11]and other semiconductors materials with suitable band alignment.[12,13] Among various methods, the uses of metal nanoparticles supported metal oxide based semiconductor nanocomposites have received great attention to boost the photophysical studies.[14–18]

Various oxide based semiconductors nanomaterials such as ZnO,[19] ZrO_2,[20] SnO_2,[21] CeO_2,[22] WO_3,[22] VO_2,[23] NiO,[24] and TiO_2[25] etc. have been established to be desirable materials for photocatalytic processes due to their high photosensitivity, large band gap, and chemical stability. Among these metal oxide materials, ZnO nanomaterials have attracted much interest in particular, because of ZnO is a typical n-type semiconductor metal oxide having a wide direct band gap (3.37 eV), and another most important nanomaterials for UV photodetection for the photocatalytic applications. ZnO shows higher electron mobility property compared to other wide band gap oxides.[26–28] Recent studies have demonstrated that the photocatalytic activities of semiconductor metal oxide nanomaterials are dependent on their average sizes and shapes.[29,30]Recently, metal nanoparticles decorated onto the surface of ZnO nanorods have become attractive catalysts for the degradation of various organic molecule and hydrogen generation by taking advantage of strong absorption in the UV region.[31]Pal et al.[15] fabricated ZnO nanorods decorated with gold nanoparticles of ~20 nm average size anddemonstrated the photocatalytic degradation of Rhodamine 6G. Meng et. al.[32] have designed Ag nanospheres onto the side surface and the top ends of large-scale vertically aligned cone-shaped ZnO nanorods 3D heterostructure. They also reported that this 3D hybrid nanostructure substrate manifests high SERS sensitivity to Rhodamine and a very low detection limit towards polychlorinated biphenyl (PCB).[77] Wu et al.[33] have successfully prepared high-density unaggregated Au NPs bonding on entire surfaces of ZnO nanorod arrays are on a conductive film/substrate. Surprisingly, this ZnO nanorod arrays/Au NPs heterostructures exhibit a photodegradation rate 8.1 times higher than that recorded for the bare ZnO nanorod arrays under UV irradiation. This enhancement resulted in the efficient separation of electron-hole pairs, which may hinder charge recombination for participation in photocatalysis.

However, synthesis of these composite Au nanoparticles decorated ZnO nanorods materials is not straightforward like

[a] K. K. Haldar, R. Biswas
Department of Chemical science, School of Basic and Applied Science, Central University of Punjab, 151001-Bathinda, Punjab, India
E-mail: cskkh@cup.ac.in
[b] S. Tanwar, T. Sen
Institute of Nano Science and Technology, 160062- Mohali, Punjab
[c] J. Lahtinen
Department of Applied Physics, Aalto University School of Science, FI-00076 Aalto, Finland

Supporting information for this article is available on the WWW under https://doi.org/10.1002/slct.201801234

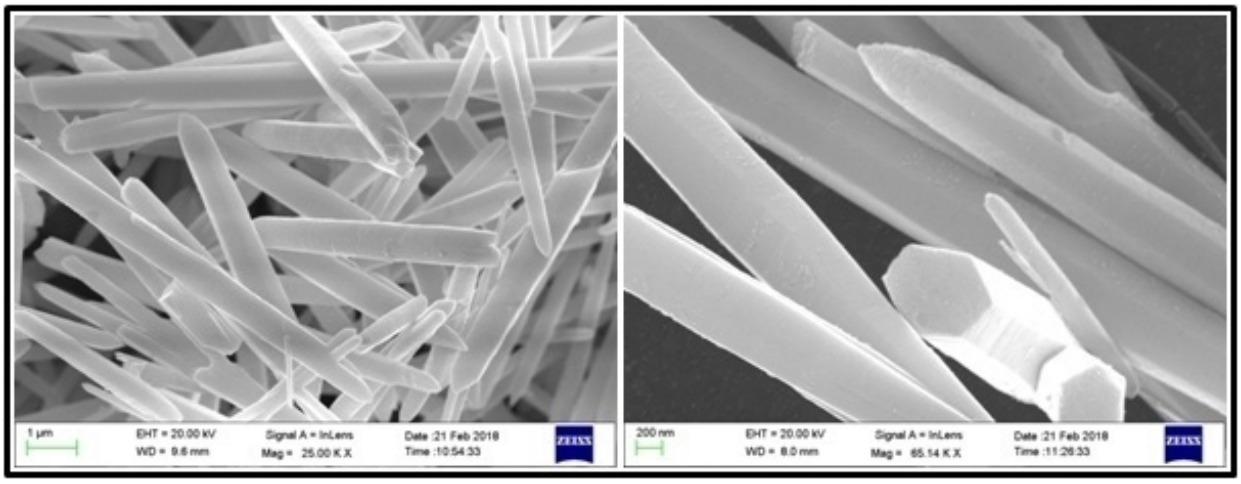

Figure 1. Shows the SEM image of Au nanoparticles embedded ZnO nanorods prepared by one-pot chemical synthesis.

Au or ZnO nanostructures; rather, it needs a more selective approach to bring both their counterparts together. For example, the ZnO nanorods parts are synthesized at a higher temperature and Au nanoparticles were nucleated via the colloidal deposition route with polyvinyl alcohol.[34,35]However, the situation remains complicated for the simultaneous nucleation and growth of the Au nanoparticles on ZnO nanorods surfaces which require a high-temperature reaction system. To best our knowledge, there is no report till date on Au nanoparticles embedded ZnO nanorods composite structure synthesized in one pot via a hydrothermal process.

Here, we have proposed to fabricate Au nanoparticles embedded ZnO nanorods composite nanostructures following the hydrothermal processand citrate reduction methods, simultaneously. These Au nanoparticles embedded ZnO composite nanostructures then manifest excellent UV-visible light directed photocatalytic performance for the photodegradation of an organic molecule such as MB in aqueous solution. Such metal-semiconductor hybrid nanostructures should have great potentials for photocatalytic properties, nonlinear optical properties, photovoltaic devices, and chemical sensors.

2. Results and discussion

The composite of Au nanoparticles embedded ZnO nanorods were prepared by one-pot growth in the colloidal solution. It has been found that almost all the Au nanoparticles embedded ZnO composite nanorods, Au nanoparticles are attached to the ZnO nanorods surface. Figure 1 represents a typical SEM image of the as-prepared Au nanoparticles embedded ZnO nanorods. The SEM clearly reveals the formation of rod-like nanostructures of faceted surface planes, in which Au nanoparticles attached. Thus the formation of Au nanoparticles on the surface of ZnO nanorods is evident from the SEM images. Again, we have confirmed the presence of Au in the Au nanoparticles embedded ZnO nanorods composite nanostructure via TEM study. The TEM observation is continual with the SEM observation. Figure 2 depicts a typical bright field TEM image of the as-synthesized composite structure in which spherical Au nanoparticles are on the surface of ZnO nanorods with an average diameter of about 160–200 nm and length 3.2-3.5 µm. Figure 2a reveals a wide view of the TEM images showing Au nanoparticles embedded ZnO nanorods. Without size sorting, the one-dimensional composite nanocrystals obtained here shows good monodispersity. The Au nanoparticles embedded ZnO nanorods composite structures possess a highly crystalline structure. In addition, the TEM images of higher magnification (Figure 2b & c) affirm that the diameter of the attached Au nanoparticles about ~8-10 nm. Overall, the Au nanoparticles in all the composite structure of Au embedded ZnO nanorods are uniform in morphology. It was noticed by HRTEM images (Figure 2d) that distinct Au nanoparticles is attached to ZnO nanorod surface. Figure 2e shows the selected-area electron diffraction (SAED) pattern for Au nanoparticles embedded ZnO nanorods composite nanostructure. The presence of the (101), (100), (102), and (110) planes for ZnO and (200) and (220) planes for Au again corroborates the formation of hexagonal ZnO (JCPDS card no. 36-1451) and face center cubic Au (JCPDS card no. 98-000-0230), respectively. Additionally, energy dispersive spectroscopy (EDS) verifies the presence of the elements Au, Zn, and O (as shown in Figure S1) in the Au nanoparticles embedded ZnO nanorods. Here, the ethylenediamine plays an important role in controlling the formation of rod-shaped ZnO. The chelating ligands ethylenediamine present in the reaction mixture may serve as consumer to Zn^{2+} cations constraining the spiral growth of the rods and directed the growth of the ZnO nanorods.[36]

The Au nanoparticles embedded ZnO nanorods composite nanostructure formation process was monitored via FT-IR studies of the ZnO nanorods in presence of Au embedded samples (Figure S2). It is reported that the reduction of Au^{3+} to Au^{0} occurs by tri-sodium citrate present in the growth solution at boiling temperature.[37] Thus, we believe that a similar situation would occur in the present study. The ionized sodium

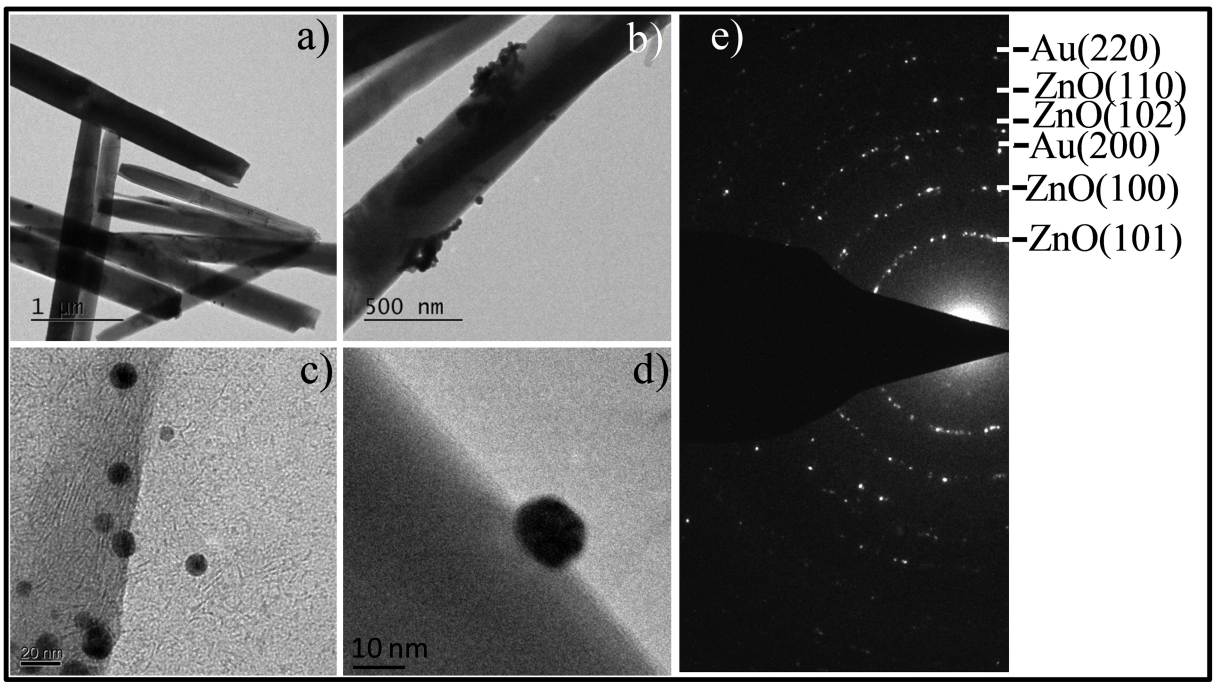

Figure 2. Typical TEM image of Au nanoparticles embedded ZnO nanorods in wide view (a and b) and high magnification (c and d). (e) Shows the selected-area electron diffraction (SAED) pattern for Au nanoparticles embedded ZnO nanorods composite nanostructure.

citrate molecules reduce Au^{3+} to Au^{0} nanoparticles in reaction medium, and it stabilizes the Au nanoparticles serving as capping agent.[37] Next, free carboxyl group of citrate ions get bonded with the Zn atoms of ZnO nanorods by chelating through bridging between the Zn atoms and the carboxyl group of citrate along with Au and this result in attachment of Au onto the ZnO surface (details in Supporting Information).[15]

For further information regarding the crystalline structure and identify the crystal phase of Au nanoparticles embedded ZnO nanorods, we have analyzed the powder X-ray diffraction (XRD) study of ZnO nanorods in presence and absence of Au. Figure 3 depicts the XRD pattern of ZnO NRs and Au nanoparticles embedded ZnO nanorods. The strong peaks appear at 31.8°(100), 34.3°(002), 36.3° (101), 47.6°(102) and 56.6°(110) (Figure 3a) clearly indicate that the as-prepared ZnO nanorods have hexagonal structure (JCPDS card no. 36-1451). On the other hand, for the Au nanoparticles embedded ZnO nanorods, we have found one more additional peak at 38.2° (Figure 3b) which corresponds to (111) plane of face center cubic Au (JCPDS card no. 98-000-0230). This result demonstrates the formation of highly crystalline Au nanoparticles embedded ZnO composite nanorods. This is in good agreement with the SAED analysis (Figure 2e). In addition, no other crystalline impurities and no remarkable diffraction peak shifting were observed.

To further study the composition of composite nanostructures, we carried out XPS measurements. Figure 4 shows the XPS spectra of Au, Zn, and O. The energy calibration was made using the Au 4f 7/2 peak at 84.0 eV. All decompositions were made with Casa XPS using GL(m) peaks (product of m% Lorenztian and 100-m % Gaussian). The Au 4d area exhibits the 4d 5/2 and 4d 3/2 peaks at 335.4 eV and 353.5 eV (Figure 4a). Only one but broad (FWHM 4.5 eV) GL(70) component is needed in the deconvolution. The relative concentration of Gold is 3.5 at-% based on the Au 3d 5/2 peak.

In the Zn 2p area the 2p3/2 and 2p1/2 peaks are visible. Both indicate only one GL(80) component (FWHM 1.5 eV) with binding energies of 1022.1 eV and 1045.2 eV (Figure 4b). The binding energy of the 2p3/2 cannot be used to identify the chemical state since both metallic Zn (0) and Zn(II) oxide have values between 1021 eV to 1022 eV.[38,39] However, the chemical state can be identified using the Auger parameter calculated using the Zn 2p3/2 peak and the LMM Auger peak. The Zn LMM Auger spectrum has a main peak at 498.5 eV and a shoulder at 495.1 eV when GL(30) peaks are used (Figure S3). The Auger parameter calculated using the main LMM peak gives a value of 2010.2 eV corresponding to Zn(II) oxide.[38] The relative concentration of Zinc is 39 at-% based on the 2p3/2 peak. The most intense Gold peak, Au 4f, overlap heavily with Zn 3d and we decided not to use those peaks to estimate the concentrations. However, it is still possible to see that the Au 4f7/2 peak is narrow (FWHM 0.74 eV) and has only one component (Figure 4c).

The O1s spectrum has two components that can be assigned to oxide at 530.9 eV and hydroxide at 532.5 eV (Figure 4d). The relative concentrations for oxide is 44 at-% and hydroxide 14 at-% based on deconvolution with two GL(60) peaks.

Figure 5 shows the absorption spectra of aqueous solutions of pure Au nanoparticles (Au nanoparticles were synthesized in absence of Zn precursor under similar condition), pure ZnO

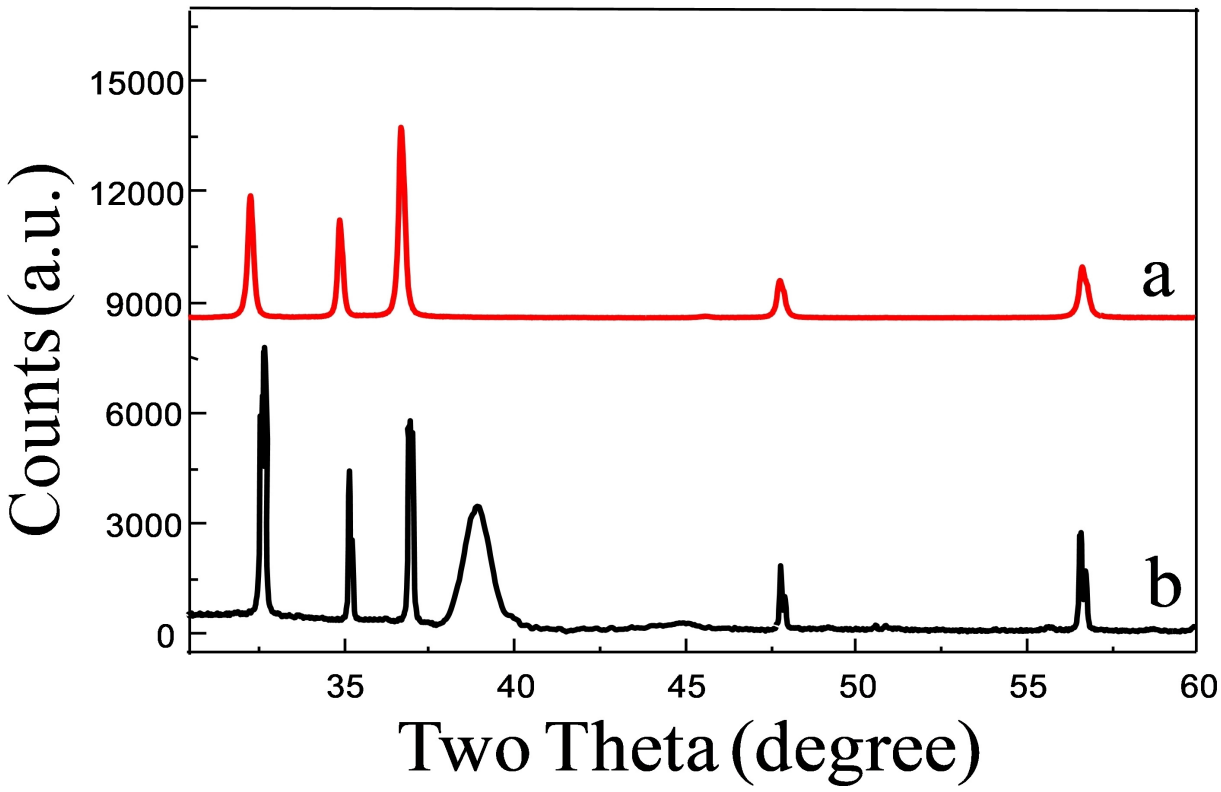

Figure 3. XRD pattern of (a) ZnO and (b) Au nanoparticles embedded ZnO nanorods.

nanorods (ZnO nanorods were synthesized in absence of Au precursor under similar condition), and Au nanoparticles embedded ZnO nanorods. The absorption spectra of both Au and ZnO change significantly upon forming directly coupled Au embedded ZnO nanorods composite structures. The plasmon bands centered at 521 and 552 nm are for pure Au and Au nanoparticles embedded ZnO nanorods, respectively. The surface plasmon band is shifted from 521 to 552 nm for Au nanoparticles embedded ZnO nanorods. The absorption peaks at 372 and 361 nm are due to excitonic band[5] for bare ZnO nanorods and Au nanoparticles embedded ZnO nanorods, respectively. The blue shifting of the excitonic band (ZnO) with respect to bare ZnO nanorods (372 nm) is obviously due to the attachment of Au nanoparticles on ZnO nanorods. As reported earlier, the high dielectric constant of the TiO_2 and SnO_2 shell on Au causes a red shift in the plasmon absorption of the Au core.[40,41] This shifting of plasmon absorption band is exploited to monitor the concentration of electrons in the Au core. It is well-known that the Fermi levels of two components equilibrate when metal nanoparticles come in contact with a charged semiconductor.[42] The Fermi level of Au is more positive ($E_F = 0.4$ V vs NHE) than the conduction band energy of ZnO ($E_{CB} = -0.5$ V vs NHE), therefore, the charge transfer from the excited ZnO to Au nanoparticles would be thermodynamically favorable.[43] The processes that lead to storage of electrons in the Au core are summarized below.

$$ZnO + hv \longrightarrow ZnO\,(\bar{e}+h^+)$$

$$ZnO\,(\bar{e}+h^+) + Au \longrightarrow Au\,(\bar{e}) + ZnO\,(h^+)$$

The photogenerated electron separation was further confirmed by comparing the photoluminescence (PL) spectra of the ZnO nanorods and Au nanoparticles embedded ZnO nanorods composite nanostructure. The characteristics of the PL spectra of the Au nanoparticles embedded ZnO nanorods composites were very analogous to bare ZnO nanorods (Figure 6). However, in case of Au nanoparticles embedded ZnO nanorods composites; the intensity of both the emission bands was much lower emission intensity than the corresponding bare ZnO nanorods. This PL intensity quenching arises due to the incorporation of Au nanoparticles on ZnO nanorods surface.[44] It is already reported that when metal and semiconductor has a direct connection, then electron transfer occurs from a conduction band of the semiconductor to the Fermi level of metal which are in low lying (Scheme 1).[45]

To further confirm the charge transfer between Au nanoparticles and ZnO nanorods, we have measured the photocurrent response of ZnO nanorods and Au nanoparticles embedded ZnO nanorods composite counterpart electrodes by inserting them in a photoelectrochemical cell. The photocurrent responses of ZnO nanorods and Au nanoparticles embedded ZnO nanorods composite structures were shown in Figure 7, under illumination of light irradiation. Both of them shows quick response regarding the on/off cycle of light

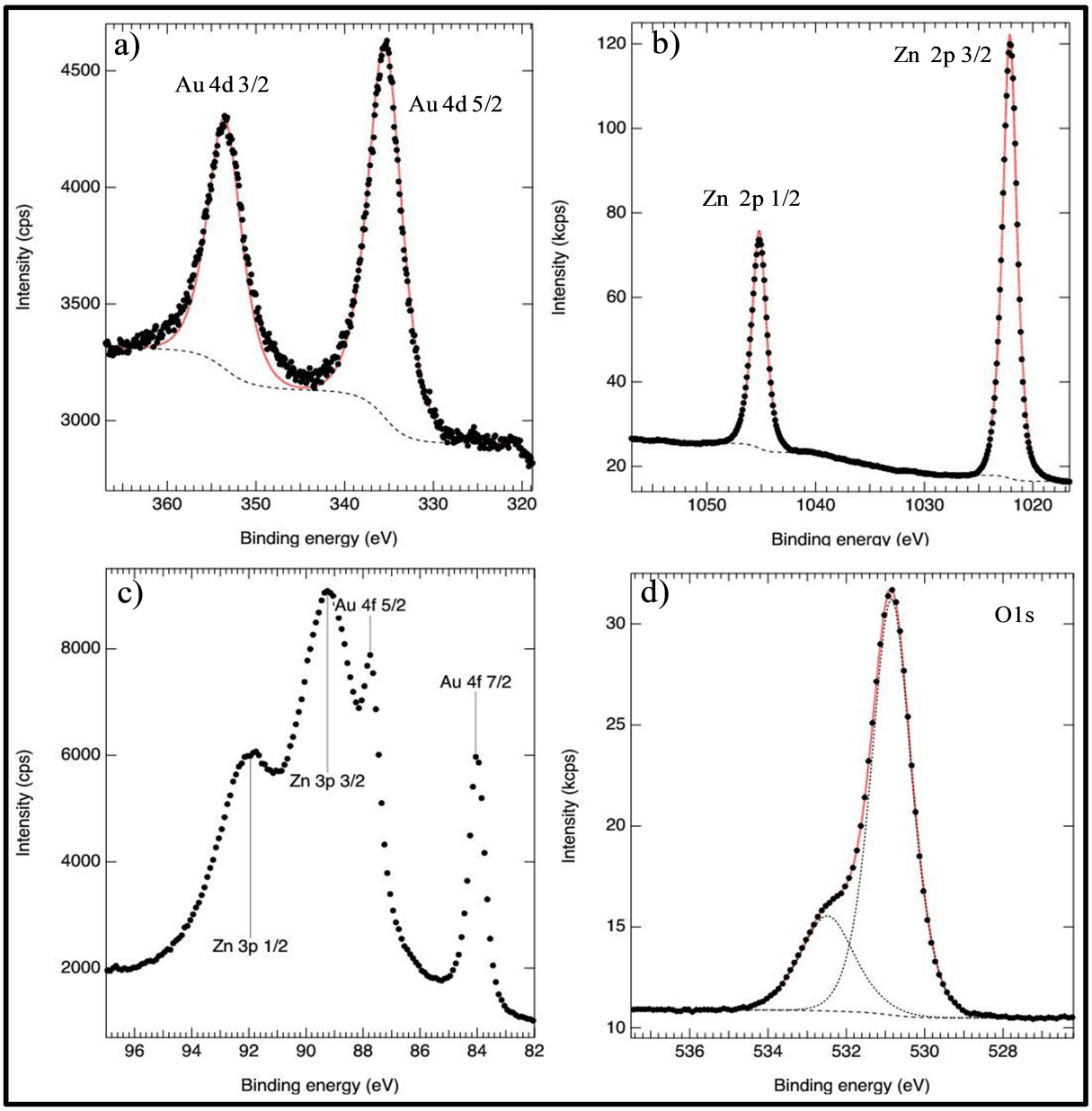

Figure 4. XPS spectra of (a) Au 4d and (b) Zn 2p (c) combined Au 4f and Zn 3p and (d) O 1s in Au nanoparticles embedded ZnO composite nanorods.

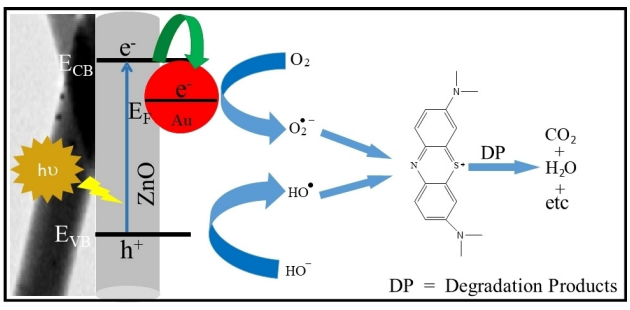

Scheme 1. Schematic presentation of the degradation process of Methylene Blue under visible light by Au nanoparticles embedded ZnO composite nanorods.

characteristic the electron transfer process from ZnO nanorods to Au nanoparticles. The result clearly demonstrates that the photocurrent response of Au nanoparticles embedded ZnO nanorods is higher compared to bare ZnO nanorods, indicating the improvement in photocurrent generation due to electron transfer from ZnO nanorods to Au nanoparticles by enhancing the lifetime of photogenerated electrons. It is believed that the electron migration mechanism from the photoexcited ZnO surface to the electron deficient Au is responsible for photocurrent generation.[46,47] Thus, the enhancement of the photoresponse speed can widen the opportunity of exploiting Au nanoparticles and ZnO nanorods composite nanostructure for superior photocatalytic activities.

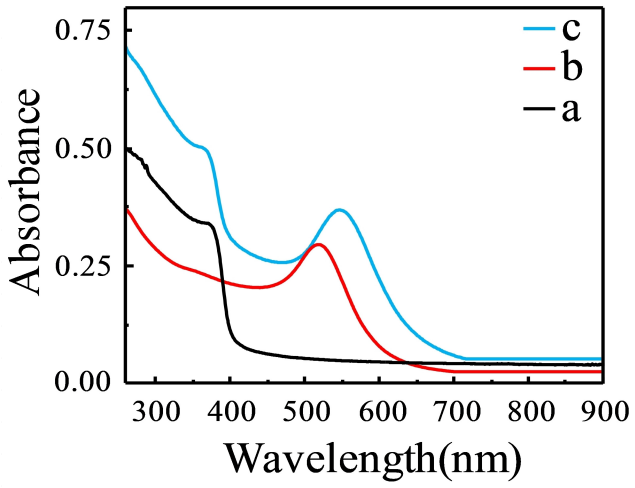

Figure 5. Absorbance spectra of (a) Pure ZnO nanorods, (b) Au nanoparticles and (c) Au nanoparticles embedded ZnO composite nanorods.

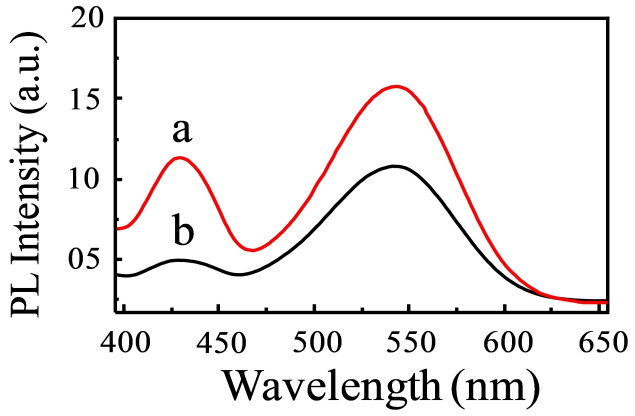

Figure 6. PL spectra of (a) ZnO and (b) Au nanoparticles embedded ZnO nanorods.

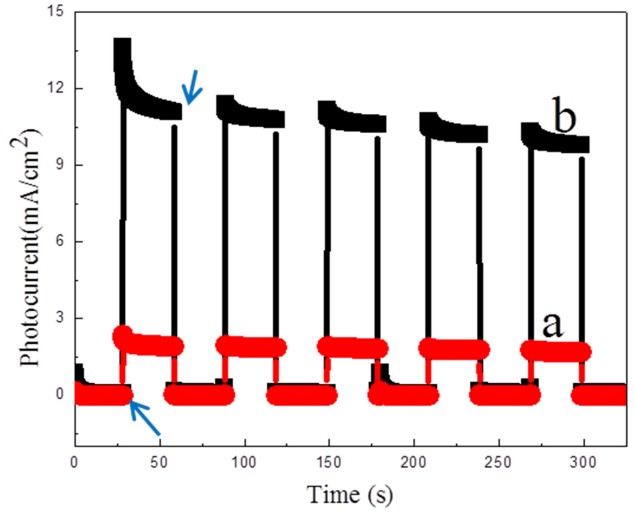

Figure 7. Photocurrent spectra of (a) ZnO and (b) Au nanoparticles embedded ZnO nanorods.

For a better understanding of the origin of the commendable catalytic performance of Au nanoparticles embedded ZnO nanorods composite nanostructure, and to interpret the PL results, we explored electrochemical impedance spectroscopy (EIS) investigation. Figure 8 shows the electrochemical impedance spectra of the ZnO nanorods and Au nanoparticles embedded ZnO nanorods composite nanostructure. EIS result depicts that the smaller impedance semicircle radius is observed for Au nanoparticles embedded ZnO nanorods composite nanostructure with respect to bare ZnO nanorods. This result indicatesthat the charge recombination rate is decreased after attachment of Au nanoparticles on ZnO nanorods surface compared to bare ZnO nanorods and electron transfer ability of Au nanoparticles on ZnO nanorods composite nanostructure enhances. This believed that upon favorable alignment of the Fermi level of Au and the conduction bands of ZnO, a cascade system was formed between the Au and ZnO heterojunctions, which facilitated the efficient charge transportation across the interface of Au nanoparticles embedded ZnO nanorods composite nanostructure. Thus, Au deposition on ZnO nanorods significantly hindered the recombination rate of the photoinduced charge carriers which leads to an excellent visible light directed photocatalytic application of Au nanoparticles embedded ZnO nanorods composites. This indicates the persistence of our EIS results, which also support the photoluminescence analysis. Therefore, a magnificent ability of photocatalytic activity is predictable at the surfaces of Au nanoparticles embedded ZnO nanorods composite nanostructure. A series of photocatalytic experiments were performed in this work to examine the photocatalytic properties of the as-synthesized Au nanoparticles embedded ZnO nanorods composite nanostructure.

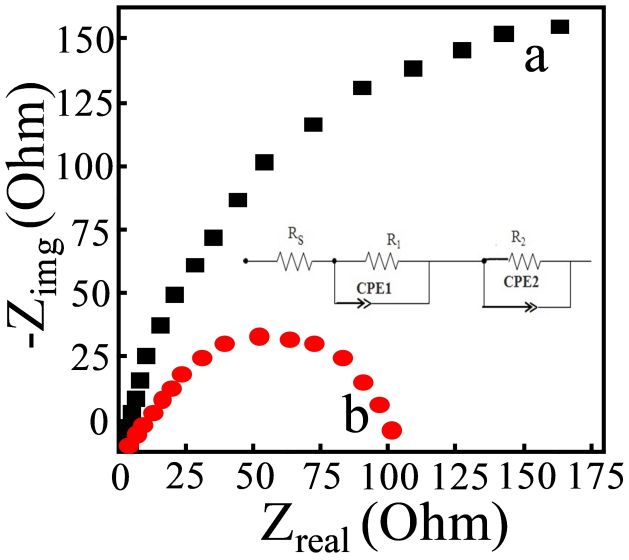

Figure 8. EIS spectra of (a) ZnO and (b) Au nanoparticles embedded ZnO nanorods.

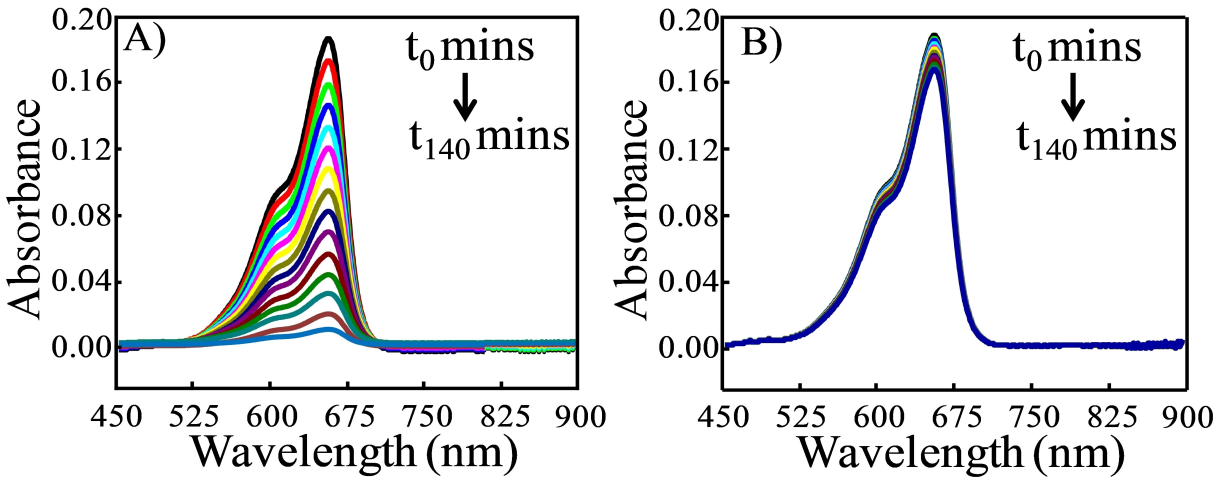

Figure 9. The absorbance spectral changes of MB solution in the presence (A) Au nanoparticles embedded ZnO composite nanorods and (B) ZnO nanorods.

2.1. Photocatalytic activity

Methylene Blue (MB), a typical dye that can be decomposed by hydroxyl radicals[48] was used as the experiment pollutant to monitor the photocatalytic oxidation progress for Au nanoparticles embedded ZnO nanorods composite nanostructure. The time-dependent UV-visible spectra of MB solutions under UV-visible light illumination in the presence of Au nanoparticles embedded ZnO nanorods composite nanostructures were shown in Figure 9A. MB dye shows a major absorption band at 663 nm in aqueous solution. It is found that the absorbance of MB is gradually reduced with increased UV irradiation time for the Au nanoparticles embedded ZnO nanorods composite nanostructure. It clearly shows that the process is slower in the case of ZnO nanorods (Figure 9B). MB–Au nanoparticles control reaction, in which tri-sodium citrate (TSC) capped Au particles of nearly 10 nm in diameter were used, is shown in Supporting Information (S4). ZnO nanorods and Au nanoparticles embedded ZnO nanorods composite nanostructures are tested for 140 min under identical conditions. It is found that 95.7% of MB dye is degraded by the Au nanoparticles embedded ZnO nanorods composite nanostructure after 140 min UV irradiation, whereas 14.7% degradation is observed in the case of ZnO nanorods. The decomposition of MB dye under the same UV irradiation condition is negligible in the presence of Au NPs and absence of both ZnO nanorods and Au nanoparticles embedded ZnO nanorods composite nanostructure. Therefore, the large reduction of MB dye absorption in the MB/Au nanoparticles embedded ZnO nanorods composite nanostructure solution can be attributed to a photocatalytic effect that happens due to the presence of the Au nanoparticles embedded ZnO nanorods composite nanostructure. Degradation rate k_D is calculated using following equation:

$$k_D = (A_0\text{-}A)/A \quad (1)$$

where A_0 and A are the initial absorbance and the sample absorbance, respectively. The kinetic profiles of degradation of MB under UV light wasalso investigated. The photodegradation of MB follows apparently first-order kinetics. Its kinetics can be expressed as $ln(I_0/I_t) = kt$, where k is the apparent reaction rate constant, I_0 is the concentration of MB at adsorption equilibrium, and I_t is the residual concentration of MB at different illumination time intervals. Figures 10A and 10B show the photodegradation of MB in terms of absorption spectra and as a function of irradiation time in the presence of Au nanoparticles embedded ZnO nanorods composite nanostructure and ZnO nanorods, respectively. The intersection of these two curves (I_t/I_0 and 1-I_t/I_0) shows the half-life of MB, which is the time taken for the concentration of MB to decrease by half.[49] The concentration of MB has decreased by half after 76.4 min and the degradation efficiency has reached 95.7% after 140 min while for ZnO nanorods, the efficiency was only nearly 14.7% after 140 min. The lifetime of a catalyst is an important parameter for any catalytic process because of its further use for a long span of time leading to a significant cost diminution. For this reason, the Au nanoparticles embedded ZnO nanorods composite catalyst was recycled, which indicate a slowdown in efficiency only from 100% (first run) to 94.1% (11th run) as shown in Figure S5. These results suggest that Au nanoparticles embedded ZnO nanorods composite catalyst can sustaineffective and reusable under UV light. The mechanism of photocatalysis can be summarized as follows:

$$ZnO + h\nu \longrightarrow ZnO\ (\bar{e} + h^+)$$

$$Au^0 + e^- \longrightarrow Au^-$$

$$Au^- + O_2 \longrightarrow Au^0 + O_2^{\bullet -}$$

$$H_2O + h^+ \longrightarrow HO^{\bullet} + H^+$$

$$HO^{\bullet} + MB \longrightarrow \text{Degradation products of MB}$$

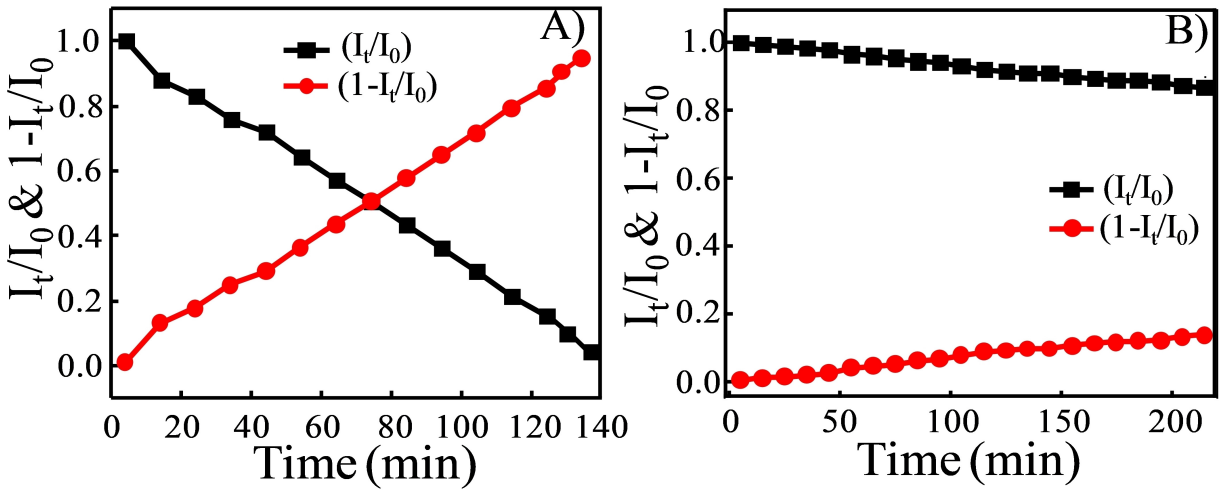

Figure 10. The intersection of these two curves (I_t/I_0 and 1- I_t/I_0) shows the half-life of MB in presence of (A) Au nanoparticles embedded ZnO composite nanorods And (B) ZnO nanorods under UV light, which the time is taken for the concentration of MB to decrease by half.

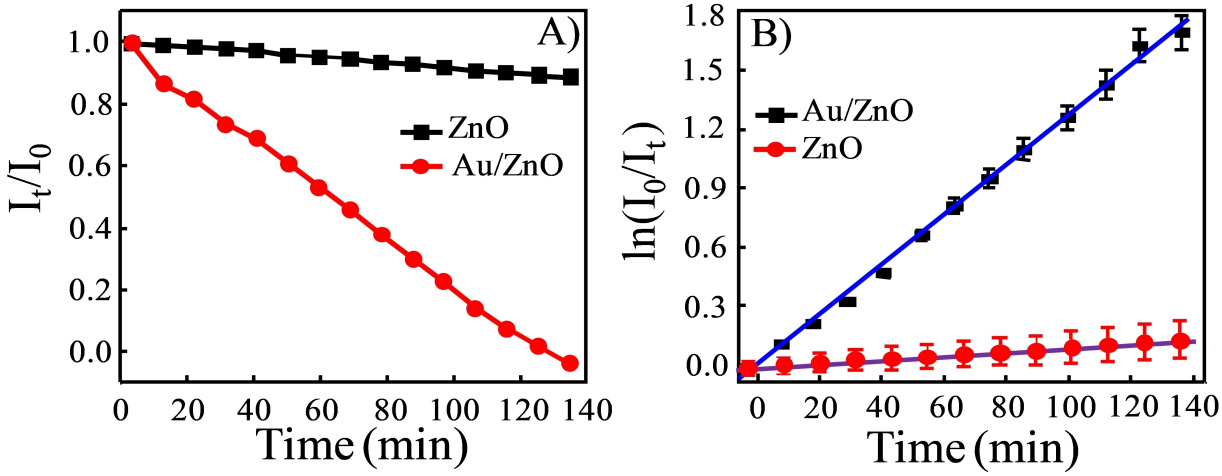

Figure 11. (A) Photodegradation and (B) rate of photodegradation of MB dye in the presence of ZnO nanorods and Au nanoparticles embedded ZnO composite nanorods under UV light.

Figure 11A and 11B show a linear relationship between (I_t/I_0) or $\ln(I_0/I_t)$ and reaction time (t), indicating that the photodegradation of MB follows a first-order kinetics model. The apparent rate constants as kinetic evidence for the samples are determined as 0.0025 and 0.015 min^{-1} for ZnO nanorods and Au nanoparticles embedded ZnO nanorods composite nanostructure, respectively. Thus, the photocatalytic activity significantly enhances due to Au nanoparticles décor ation on ZnO nanorods surface. These results clearly demonstrate that the Au nanoparticles embedded ZnO nanorods composite nanostructures have commendable improved photocatalytic activities in comparison with ZnO nanorods. Thus, the Au nanoparticles embedded ZnO nanorods composite nanostructure improve the separation of photogenerated electron-hole pairs due to the potential energy differences between Au and ZnO, thus enhancing the photocatalytic activity.

Conclusion

In summary, a novel chemical approach for the one-pot synthesis of Au nanoparticles embedded ZnO nanorods composite nanostructure and its formation chemistry have been discussed. Au nanoparticles embedded ZnO nanorods composite nanostructure caused the material to exhibit significant improvement in the photocatalytic activity. The examination of photoreduction ability shows that the Au nanoparticles embedded ZnO nanorods composite structure possess higher photoreduction ability than the bare ZnO nanorods for the degradation of MB under UV-light irradiation due to the enhanced separation efficiency of photogenerated electron-hole pairs and exhibited excellent stability (about 5% loss after 11th cycles). This is not only because of the low internal resistance but also due to electrons tapping and accumulation between Au nanoparticles and ZnO nanorods

interfacial Schottky barrier.[42,50] The design of new optical-based materials based on metal-semiconductor heterostructures has opened up new possibilities for photocatalytic and optoelectronic applications. Although many issues are to be addressed, the general interest in metal-semiconductor heterostructures is expected to grow in coming years because applications are still in the embryonic stage.

Supporting Information

Experimental details, EDS Line scan mappings for elements O, Zn, and Au in Au/ZnO composite, FTIR spectra of Au nanoparticles embedded ZnO composite nanorods, the Zn LMM Auger spectrum, photocatalyst loading optimization and photocatalytic cycle for its reusability are available in supporting information.

Acknowledgment

We acknowledge the provision of facilities of Aalto University at OtaNano - Nanomicroscopy Center (Aalto-NMC). This work was financially supported by the UGC Start-up grant.

Conflict of Interest

The authors declare no conflict of interest.

Keywords: Au/ZnO · composite · nanorods · Photocatalyst

[1] X. Chen, S. Shen, L. Guo, S. S. Mao, *Chem. Rev. (Washington, DC, U. S.)* **2010**, *110*, 6503.
[2] H. Park, H.-i. Kim, G.-h. Moon, W. Choi, *Energy Environ. Sci.* **2016**, *9*, 411.
[3] R. Costi, A. E. Saunders, E. Elmalem, A. Salant, U. Banin, *Nano Lett.* **2008**, *8*, 637.
[4] K. K. Haldar, G. Sinha, J. Lahtinen, A. Patra, *ACS Appl. Mater. Interfaces* **2012**, *4*, 6266.
[5] K. K. Haldar, T. Sen, *J. Colloid Interface Sci.* **2016**, *484*, 263.
[6] K. K. Haldar, V. Y. Muley, S. Datar, A. Patra, *Gold Bull. (Berlin, Ger.)* **2017**, *50*, 105.
[7] K. K. Haldar, S. Kundu, A. Patra, *Appl. Phys. Lett.* **2014**, *104*, 063110/1.
[8] B. Gao, Y. Lin, S. Wei, J. Zeng, Y. Liao, L. Chen, D. Goldfeld, X. Wang, Y. Luo, Z. Dong, J. Hou, *Nano Res.* **2012**, *5*, 88.
[9] T.-T. Yang, W.-T. Chen, Y.-J. Hsu, K.-H. Wei, T.-Y. Lin, T.-W. Lin, *J. Phys. Chem. C* **2010**, *114*, 11414.
[10] G. Manna, R. Bose, N. Pradhan, *Angew. Chem., Int. Ed.* **2014**, *53*, 6743.
[11] H. Chauhan, Y. Kumar, J. Dana, B. Satpati, H. N. Ghosh, S. Deka, *Nanoscale* **2016**, *8*, 15802.
[12] V. Chakrapani, K. Tvrdy, P. V. Kamat, *J. Am. Chem. Soc.* **2010**, *132*, 1228.
[13] L. Wu, J. Xing, Y. Hou, F. Y. Xiao, Z. Li, H. G. Yang, *Chem. - Eur. J.* **2013**, *19*, 8393.
[14] K. Kaehler, M. C. Holz, M. Rohe, J. Strunk, M. Muhler, *ChemPhysChem* **2010**, *11*, 2521.
[15] M. D. L. Ruiz Peralta, U. Pal, R. S. Zeferino, *ACS Appl. Mater. Interfaces* **2012**, *4*, 4807.
[16] J.-J. Wu, C.-H. Tseng, *Appl. Catal., B* **2006**, *66*, 51.
[17] P. Zhai, C.-C. Lee, Y.-H. Chang, C. Liu, T.-C. Wei, S.-P. Feng, *ACS Appl. Mater. Interfaces* **2015**, *7*, 2116.
[18] L.-M. Chen, L.-B. Luo, Z.-H. Chen, M.-L. Zhang, J. A. Zapien, C.-S. Lee, S.-T. Lee, *J. Phys. Chem. C* **2010**, *114*, 93.
[19] Y. J. Jang, C. Simer, T. Ohm, *Mater. Res. Bull.* **2006**, *41*, 67.
[20] V. R. Reddy, D. W. Hwang, J. S. Lee, *Korean J. Chem. Eng.* **2003**, *20*, 1026.
[21] D.-F. Zhang, L.-D. Sun, J.-L. Yin, C.-H. Yan, *Adv. Mater. (Weinheim, Ger.)* **2003**, *15*, 1022.
[22] G. R. Bamwenda, T. Uesigi, Y. Abe, K. Sayama, H. Arakawa, *Appl. Catal., A* **2001**, *205*, 117.
[23] Y. Wang, Z. Zhang, Y. Zhu, Z. Li, R. Vajtai, L. Ci, P. M. Ajayan, *ACS Nano* **2008**, *2*, 1492.
[24] J.-J. Zou, C.-J. Liu, Y.-P. Zhang, *Langmuir* **2006**, *22*, 2334.
[25] S.-H. Lee, Y. Park, K.-R. Wee, H.-J. Son, D. W. Cho, C. Pac, W. Choi, S. O. Kang, *Org. Lett.* **2010**, *12*, 460.
[26] S. H. Ko, D. Lee, H. W. Kang, K. H. Nam, J. Y. Yeo, S. J. Hong, C. P. Grigoropoulos, H. J. Sung, *Nano Lett.* **2011**, *11*, 666.
[27] C. Klingshirn, *Phys. Status Solidi B* **2007**, *244*, 3027.
[28] W. Dai, X. Pan, S. Chen, C. Chen, Z. Wen, H. Zhang, Z. Ye, *J. Mater. Chem. C* **2014**, *2*, 4606.
[29] G. Cernuto, N. Masciocchi, A. Cervellino, G. M. Colonna, A. Guagliardi, *J. Am. Chem. Soc.* **2011**, *133*, 3114.
[30] A. Kar, S. Sain, S. Kundu, A. Bhattacharyya, S. Kumar Pradhan, A. Patra, *ChemPhysChem* **2015**, *16*, 1017.
[31] Y. Wei, L. Ke, J. Kong, H. Liu, Z. Jiao, X. Lu, H. Du, X. W. Sun, *Nanotechnology* **2012**, *23*, 235401/1.
[32] H. Tang, G. Meng, Q. Huang, Z. Zhang, Z. Huang, C. Zhu, *Adv. Funct. Mater.* **2012**, *22*, 218.
[33] T.-H. Yang, L.-D. Huang, Y.-W. Harn, C.-C. Lin, J.-K. Chang, C.-I. Wu, J.-M. Wu, *Small* **2013**, *9*, 3169.
[34] J. Strunk, K. Kaehler, X. Xia, M. Comotti, F. Schueth, T. Reinecke, M. Muhler, *Appl. Catal., A* **2009**, *359*, 121.
[35] M. Comotti, W.-C. Li, B. Spliethoff, F. Schueth, *J. Am. Chem. Soc.* **2006**, *128*, 917.
[36] B. Liu, H. C. Zeng, *J. Am. Chem. Soc.* **2003**, *125*, 4430.
[37] J. Kimling, M. Maier, B. Okenve, V. Kotaidis, H. Ballot, A. Plech, *J. Phys. Chem. B* **2006**, *110*, 15700.
[38] M. C. Biesinger, L. W. M. Lau, A. R. Gerson, R. S. C. Smart, *Appl. Surf. Sci.* **2010**, *257*, 887.
[39] S. Bera, S. Dhara, S. Velmurugan, A. K. Tyagi, *Int. J. Spectrosc.* **2012**, 371092.
[40] T. Hirakawa, P. V. Kamat, *J. Am. Chem. Soc.* **2005**, *127*, 3928.
[41] G. Oldfield, T. Ung, P. Mulvaney, *Adv. Mater. (Weinheim, Ger.)* **2000**, *12*, 1519.
[42] A. Wood, M. Giersig, P. Mulvaney, *J. Phys. Chem. B* **2001**, *105*, 8810.
[43] K. K. Haldar, T. Sen, A. Patra, *J. Phys. Chem. C* **2008**, *112*, 11650.
[44] J. R. Lakowicz, *Anal. Biochem.* **2005**, *337*, 171.
[45] X. Li, Y. Zhang, X. Ren, *Opt. Express* **2009**, *17*, 8735.
[46] M. N. Tahir, F. Natalio, M. A. Cambaz, M. Panthoefer, R. Branscheid, U. Kolb, W. Tremel, *Nanoscale* **2013**, *5*, 9944.
[47] P. She, K. Xu, Y. Shang, Q. He, S. Zeng, S. Yin, G. Lu, S. Liang, H. Sun, Z. Liu, *New J. Chem.* **2018**, *42*, 3315.
[48] C.-H. Wu, J.-M. Chern, *Ind. Eng. Chem. Res.* **2006**, *45*, 6450.
[49] N. Soltani, E. Saion, M. Z. Hussein, M. Erfani, A. Abedini, G. Bahmanrokh, M. Navasery, P. Vaziri, *Int. J. Mol. Sci.* **2012**, *13*, 12242.
[50] X. Zheng, X. Yan, Y. Sun, Z. Bai, G. Zhang, Y. Shen, Q. Liang, Y. Zhang, *ACS Appl. Mater. Interfaces* **2015**, *7*, 2480.

Submitted: April 24, 2018
Accepted: June 27, 2018